

**Particle size
distributions in the
tropical tropopause**

S. Iwasaki et al.

Characteristics of particle size distributions in the tropical tropopause based on optical particle counter and lidar measurements

S. Iwasaki¹, K. Maruyama², M. Hayashi³, S. Y. Ogino⁴, H. Ishimoto⁵,
Y. Tachibana^{4,6}, A. Shimizu⁷, I. Matsui⁷, N. Sugimoto⁷, K. Yamashita⁵, K. Saga³,
K. Iwamoto⁸, Y. Kamiakito⁹, A. Chabangborn¹⁰, B. Thana¹⁰, M. Hashizume¹⁰,
T. Koike¹¹, and T. Oki¹²

¹Dept. of Earth and Ocean Sciences, National Defense Academy, 1-10-20 Hashirimizu, Yokosuka, Kanagawa 239-8686, Japan.

²Dept. of Information and Systems Engineering, Kanazawa University, Kakuma-machi, Kanazawa 920-1192, Japan

³Dept. of Earth System Science, Fukuoka University, 8-19-1 Nanakuma, Jonan, Fukuoka 814-0180, Japan

⁴Inst. of Observational Research for Global Change, Japan Agency for Marine-Earth Science and Technology, 2-15 Natsushima, Yokosuka 237-0061, Japan.

⁵Meteorological Research Institute, 1-1 Nagamine, Tsukuba, Ibaraki 305-0052, Japan

Title Page

Abstract

Introduction

Conclusions

References

Tables

Figures

◀

▶

◀

▶

Back

Close

Full Screen / Esc

Printer-friendly Version

Interactive Discussion

**Particle size
distributions in the
tropical tropopause**S. Iwasaki et al.

[Title Page](#)[Abstract](#)[Introduction](#)[Conclusions](#)[References](#)[Tables](#)[Figures](#)[I◀](#)[▶I](#)[◀](#)[▶](#)[Back](#)[Close](#)[Full Screen / Esc](#)[Printer-friendly Version](#)[Interactive Discussion](#)

⁶Graduate School of Earth and Environmental Science, Tokai University, 1117 Kitakaname, Hiratsuka 259-1292, Japan

⁷National Inst. for Environmental Studies, 16-2 Onogawa, Tsukuba, Ibaraki 305-8506, Japan

⁸National Research Inst. for Earth Science and Disaster Prevention, 3-1 Tennodai, Tsukuba 305-0006, Japan

⁹Graduate School of Science, Tokai University, 1117 Kitakaname, Hiratsuka 259-1292, Japan

¹⁰Faculty of Science, Chulalongkorn University, 254 Phyathai Road, Patumwan, Bangkok 10330, Thailand

¹¹School of Engineering, The University of Tokyo, 7-3-1 Hongo, Bunkyo 113-0033, Japan

¹²Inst. of Industrial Science, The University of Tokyo, 4-6-1 Komaba, Meguro 153-8505, Japan

Received: 8 January 2007 – Accepted: 22 January 2007 – Published: 31 January 2007

Correspondence to: S. Iwasaki (iwasaki@nda.ac.jp)

Abstract

An optical particle counter (OPC) is used in conjunction with lidar measurements to examine the characteristics of the particle size distribution in cirrus cloud at the tropical tropopause (TT) over Thailand. Of 11 OPC launches, cirrus cloud was detected at 10–15 km high on 7 occasions, cirrus was detected at the TT in 6 cases, and simultaneous OPC and lidar measurements were made on two occasions. Comparison of lidar and OPC measurements reveal that the cloud height of cirrus in the TT varies by several hundred meters over distances of tens kilometers; hence the height is not horizontally uniform. The mode radii of particles constituting the clouds are estimated by lidar and OPC measurements to be less than approximately $10\ \mu\text{m}$. The regression lines of the particle size distribution with and without cirrus cloud exhibit similar features at equivalent radii of $<0.7\ \mu\text{m}$. Enhancement in the integrated number concentration at radii greater than $0.7\ \mu\text{m}$ indicates that liquid particles tend to be frozen at a radius of $0.7\ \mu\text{m}$, with cirrus clouds above 10 km exhibiting similar features. In addition, common features of cirrus clouds at the TT include a local maximum in the particle size distribution at $2.0\ \mu\text{m}$ and a peak between $0.5\ \mu\text{m}$ and $1.7\ \mu\text{m}$ in the ratio of the standard deviation of count values to that of the Poisson distribution of the averaged count values. Each feature implies that all ice particles in the clouds may be nucleated by the same mechanism and particles in this size range are actively frozen at the TT. These parameters are thus good indicators for checking the results of cirrus cloud models in the TT.

1 Introduction

Subvisual cirrus clouds (SVCs), defined as cirrus with an optical thickness of less than 0.03 (Sassen and Cho, 1992), generally occur at heights of around 17 km in the tropical tropopause layer (TTL). Using data obtained in the second Stratospheric Aerosol and Gas Experiment (SAGE II), Wang et al. (1996) showed the frequency of SVC

Particle size distributions in the tropical tropopause

S. Iwasaki et al.

Title Page

Abstract

Introduction

Conclusions

References

Tables

Figures

◀

▶

◀

▶

Back

Close

Full Screen / Esc

Printer-friendly Version

Interactive Discussion

**Particle size
distributions in the
tropical tropopause**S. Iwasaki et al.

[Title Page](#)[Abstract](#)[Introduction](#)[Conclusions](#)[References](#)[Tables](#)[Figures](#)[⏪](#)[⏩](#)[◀](#)[▶](#)[Back](#)[Close](#)[Full Screen / Esc](#)[Printer-friendly Version](#)[Interactive Discussion](#)

occurrence can exceed 50% over the warm water pool. Winker and Trepte (1998) examined SVCs observed in the Lidar In-space Technology Experiment (LITE) mission and reported that the horizontal scale of the SVCs was approximately 500 km. The effects of SVCs have been studied by many researchers. Wang et al. (1996) also showed that SVCs significantly affect the radiation budget, and Eguchi and Shiotani (2004) reported that SVCs lead to the dehydration of air entering the stratosphere. Gettelman et al. (2004) reported on the basis of computations that water vapor is the most important contributor to the TTL radiation balance where the water vapor content is affected by the presence of SVCs. Therefore, SVCs are considered to play an important role in controlling radiation and water vapor content in the TTL. Historical and recent studies on SVCs are summarized in the work of Lynch et al. (2002, Chapter 12) and Hasebe et al. (2005).

Boehm and Verlinde (2000) were the first to report an analysis of SVCs on the basis of combined lidar and radiosonde data, and concluded that SVCs are generated by negative temperature anomalies induced by Kelvin waves. Comstock et al. (2002) analyzed the same data over 7 months, including the month analyzed by Boehm and Verlinde (2000), and determined that high cirrus with a cloud base of greater than 15 km does not coincide with negative temperature anomalies as often as found by Boehm and Verlinde (2000). Iwasaki et al. (2004) and Matsuura (2005) analyzed ship-borne lidar and radiosonde data and obtained similar findings to Comstock et al. (2002). To evaluate these hypotheses, extensive observations and analyses of SVCs using lidar and radiosonde instruments have been performed by many researchers.

Jensen et al. (1996) and Jensen and Pfister (2004) investigated the SVC generation mechanism through calculations of cloud microphysics in the TTL using Lagrangian one-dimensional models. Their results suggest that the injection of water vapor by deep convection is required to explain the observed humidity at the TTL.

To improve the numerical models of SVC generation and to validate computational results, observations of cloud condensation nuclei (CCN) and SVC particles are important. However, few studies have investigated aerosol and cloud particles

Particle size distributions in the tropical tropopause

S. Iwasaki et al.

[Title Page](#)[Abstract](#)[Introduction](#)[Conclusions](#)[References](#)[Tables](#)[Figures](#)[⏪](#)[⏩](#)[◀](#)[▶](#)[Back](#)[Close](#)[Full Screen / Esc](#)[Printer-friendly Version](#)[Interactive Discussion](#)

at temperatures in the range of $-80\text{ }^{\circ}\text{C}$ in the tropics. Peter et al. (2003) examined the microphysics of ultrathin tropical tropopause clouds by airborne lidar observations and particle counter measurements over the Indian Ocean, and presented a summary of the cloud morphology. Kojima et al. (2004) reported the chemical components of aerosols in the TTL based on transmission electron microscopy (TEM) measurements. Both of these studies involved airborne measurements, which are expensive to conduct and are not suitable for measuring the vertical profiles of aerosol and cloud particles. In this study, a balloon-borne optical particle counter (OPC) is used to obtain more useful measurements, coupled with simultaneous lidar measurements. The measurement campaign was conducted from April to June 2003 in Thailand (17.2°N , 99.9°E).

The specifications of the OPCs and the lidar are described in Sect. 2. Our observational results are shown in Sect. 3 and discussed them in Sect. 4. Finally, we summarize the study in Sect. 5.

2 Instruments

2.1 Optical particle counter

The OPC employed in this study provides 8 channels of detection, corresponding to radii from 0.15 to $3.5\text{ }\mu\text{m}$ assuming spherical sulfuric acid particles. The data obtained are integrated number concentrations N ($/\text{m}^3$). Figure 1 shows a schematic diagram of the OPC instrument. Particles in the ambient air are guided by a pump through the beams of laser diodes transmitting at 780 nm . The scattered light, with scattering angle of 60° and half solid angle of 44° , is detected by a photodiode via two lenses. The scattering at this angle is affected by less structural interference than other angles. The estimated particle radius is determined by

$$\Delta C_{\text{sca}} = \int_{\Delta\Omega} \frac{dC_{\text{sca}}}{d\Omega} d\Omega, \quad (1)$$

Particle size distributions in the tropical tropopause

S. Iwasaki et al.

Title Page

Abstract

Introduction

Conclusions

References

Tables

Figures

◀

▶

◀

▶

Back

Close

Full Screen / Esc

Printer-friendly Version

Interactive Discussion

where Ω denotes the solid angle. The result, particle count value, is obtained from a look-up table of ΔC_{sca} and r . The table is calculated by Mie theory assuming the particle to be a spherical sulfuric acid particle with concentration of 70 wt% (refractive index, $1.4 + i0$; Baumardner et al., 1996; Steele and Hamill, 1981). The measurement errors due to irregularities in particle shape are calculated by the finite-difference time-domain (FDTD) method (e.g., Yang and Liou 1995) as discussed in Appendix A. The minimum detectable N and the vertical resolution are approximately $1.5 \times 10^4 / \text{m}^3$ and 50 m at the TTL. The detailed OPC specifications are listed in Table 1 and presented in Hayashi et al. (1998).

All OPCs were calibrated by laboratory measurements with spherical polystyrene latex particles with refractive index of $1.59 + i0$ (e.g., Tsuchiya et al. 1996, Fig. 5). The thresholds of ΔC_{sca} for counting sulfuric acid particles (refractive index, $1.4 + i0$) were thus determined (see Appendix A, Fig. 6). The observational error of the OPCs was less than 5%.

The size distribution dn/dr (number/ $\mu\text{m}/\text{m}^3$) is derived by subtracting data on adjacent channels; e.g., dn/dr from $0.15 \mu\text{m}$ to $0.25 \mu\text{m}$ channels is calculated from the following equation.

$$\left. \frac{dn}{dr} \right|_{r=0.15 \sim 0.25 \mu\text{m}} = \frac{N|_{r=0.25 \mu\text{m}} - N|_{r=0.15 \mu\text{m}}}{0.25 - 0.15}. \quad (2)$$

As channel 8 of the OPC measures all particles larger than $3.5 \mu\text{m}$ radius, the maximum particle radius for the size distribution $dn/dr|_{r=3.5-5.0 \mu\text{m}}$ is assumed to be $5 \mu\text{m}$. Therefore, the accuracy of dn/dr for the largest particle size is not known.

Note that “particles” in this paper refer to both aerosols and cloud particles, as distinction between the two types is not possible with the present OPC. Particles detected on channel 8 are also assumed to be ice particles, as explained in Appendix B.

2.2 Lidar

The lidar used in the present study is based on a Nd:YAG laser (wavelengths are 1064 nm and 532 nm) with both transmitted energy of 20 mJ per pulse at a pulse repetition frequency of 10 Hz. The lidar return signal is received by two photomultiplier tubes at 532 nm to determine the depolarization ratio and an avalanche photodiode at 1064 nm through a 20 cm telescope. The laser was configured to fire beams for 5 min then cool down for 10 min in order to prolong the life of the flashlamp that induces the laser pulse. Each datum was obtained as the average over 5 min. The vertical resolution of lidar measurements was set at 6 m. A range of temporal and vertical resolutions could be set on the laptop computer connect to the lidar instrument.

The lidar was able to detect backscattering coefficient by gas at altitudes of up to 14 km high on a clear day at 532 nm using the 5 min average over a length of 100 m, where the backscattering coefficient β (/m/str) is defined as Eq. 3.

$$\beta = \frac{1}{4\pi} \int C_{\text{bk}}(r) \frac{dn}{dr} dr, \quad (3)$$

where $C_{\text{bk}}(r)$ denotes the backscattering cross section (m^2). The sensitivity of the instrument at 532 nm is approximately 3×10^{-7} /m/str at 14 km high.

Due to noise at 1064 nm, we analyze backscattering coefficient at 532 nm ($\beta(532)$). To calibrate the data, the lidar return was fitted to $\beta(532)$ calculated from the pressure and temperature measured by the OPC at heights of 10 km to 13 km without cloud below. Hence, the calibration corrects the attenuation below 10 km. The depolarization ratio was also fitted to the values estimated by the OPC at a height of approximately 4 km.

Particle size distributions in the tropical tropopause

S. Iwasaki et al.

Title Page

Abstract

Introduction

Conclusions

References

Tables

Figures

◀

▶

◀

▶

Back

Close

Full Screen / Esc

Printer-friendly Version

Interactive Discussion

3 Observations

3.1 Observational period and site

The observation period was from March to June in 2003. Lidar measurements were implemented throughout this period at Sri Samrong (17.16° N, 99.87°E) in Thailand. Radiosonde instruments were launched once a day adjacent to the lidar site. A total of 3 one-week intensive observation periods (IOPs) were performed from March to June. The OPC were launched in IOPs as listed in Table 2.

3.2 T_{BB}

The equivalent blackbody temperature (T_{BB}) is presented in Fig. 2 as the average value in the region $17.16 \pm 0.5^\circ \text{N}$, $99.87 \pm 0.5^\circ \text{E}$ over 2 days, where T_{BB} was measured with the geostational meteorological satellite (GMS) and the geostationary operational environmental satellite (GOES) since GMS was stopped the operation after 22 May 2003. In the figure, “O” denotes launches on which cirrus clouds were observed at the TT, and “X” denotes launches on which cirrus at the TT was not detected. Of the 11 OPC launches, clouds were detected on 6 occasions, among which 4 detections were immediately prior or following monsoon onset late in May. As the lifetime of SVCs is typically less than 1 day due to its terminal velocity (Iwasaki et al., 2004, Fig. 3), each OPC launch detected different clouds. The present results suggest that cloud at the TT tends to occur during the monsoon season.

3.3 OPC results I: Integrated number concentration

Figure 3 shows the averaged integrated number concentration $\langle N \rangle$ obtained by OPC measurements. Integrated number of particles (a,b) at 10–15 km and (c,d) at the TT ($< -75^\circ \text{C}$) under conditions of (a,c) no cloud (background aerosols) and (b,d) cloud are shown. The error bars at equivalent radius r_{eq} are calculated by the scattering

Title Page

Abstract

Introduction

Conclusions

References

Tables

Figures

◀

▶

◀

▶

Back

Close

Full Screen / Esc

Printer-friendly Version

Interactive Discussion

of irregularly shaped particles as explained in Appendix A and those at $\langle N \rangle$ are the standard deviation of Poisson distribution.

Without clouds (Figs. 3(a) and (c)), $\langle N \rangle$ decreases monotonically with regression lines of $1.5 \times 10^3 r^{-3.5} / \text{m}^3$ (10–15 km) and $4.7 \times 10^2 r^{-3.9} / \text{m}^3$ (TT), where the radius r is in micrometers. In cases when ice clouds were detected, $\langle N \rangle$ also decreases but is departs from the regression line at radii greater than approximately $0.7 \mu\text{m}$.

3.4 OPC results II: Ratio of standard deviations of count value to Poisson distribution

Figure 4 is the same as Fig. 3 but the ratio of $\sigma(\text{counts})$ and $\sigma(\text{Poisson})$ where $\sigma(\text{counts})$ denotes standard deviation of particle count values at each channel N_{raw} , raw data of OPC, and $\sigma(\text{Poisson})$ denotes that of the Poisson distribution. The plotted data are calculated according to

$$\sigma(\text{counts}) = \sqrt{\frac{1}{N} \sum_{\text{layer}}^N (N_{\text{raw}} - \langle N_{\text{raw}} \rangle)^2} \quad (4)$$

$$\sigma(\text{Poisson}) = \sqrt{\langle N_{\text{raw}} \rangle}$$

This ratio approaches unity for a vertically homogeneous cloud, and represents a useful indicator of the vertical homogeneity of the particle number.

Figure 4 shows that the ratio is lower in cases when no cloud was detected (Figs. 4a and c) than when cloud was present (Figs. 4b and d), respectively. Hence, the vertical profiles of background aerosols are relatively uniform. In addition, the average ratio over the 10–15 km altitude (Figs. 4a and b) is greater than that at the TT (Figs. 4c and d). This is because the variation of height is different, that is, 5 km depth in 4a and b and approximately 3 km depth in 4c and d, and because the ice nucleation in 4a is more active than that in 4d due to deep convection and higher temperature.

Note that there are peaks between $0.5 \mu\text{m}$ and $1.7 \mu\text{m}$ in TT when there are clouds (Fig. 4d) while the peak is not clear at a height from 10 to 15 km (Fig. 4b).

Particle size distributions in the tropical tropopause

S. Iwasaki et al.

Title Page

Abstract

Introduction

Conclusions

References

Tables

Figures

◀

▶

◀

▶

Back

Close

Full Screen / Esc

Printer-friendly Version

Interactive Discussion

3.5 OPC results III: Size distribution

Figure 5 is the same as Fig. 3 but the average particle size distributions dn/dr . It shows that particles smaller than $2.0 \mu\text{m}$ in radius are commonly present and the regression line of dn/dr for the vertical size profile of background aerosols (Figs. 5a and c) are $7.2 \times 10^3 r^{-4.3}$ and $2.7 \times 10^3 r^{-4.8}/\text{m}^3$. Aerosols at the TT are known to form the Junge layer, primarily consisting of sulfuric acid (H_2SO_4) and ammonium sulfate (e.g., Hobbs, 2000; Kojima et al., 2004, Table 2). dn/dr from 10 to 15 km high and that at TT (Figs. 5(b) and (d)) show that dn/dr for clouds decreases monotonically, with the regression lines fitting up to $1.3 \mu\text{m}$ and $0.8 \mu\text{m}$, respectively.

Of the 7 OPCs detected clouds between 10 km and 15 km, only one (1 June) involved a local maximum at $2.0 \mu\text{m}$, while no particles at $2.9 \mu\text{m}$ were detected at 10–15 km on three occasions. Figure 5d shows 6 results for cirrus clouds at the TT, of which 4 cases exhibit a local maximum at a radius of $2.0 \mu\text{m}$, and two cases show an absence of particles of radius $2.9 \mu\text{m}$ at the TT.

Note that the minimum at $2.9 \mu\text{m}$ in Figs. 5b and d is not reliable because the value of dn/dr at $4.4 \mu\text{m}$ is not accurate (see Sect. 2.1).

3.6 Comparison of lidar and OPC data

Table 2 summarizes the particle numbers and maximum β in cirrus clouds at the TT. Two simultaneous observations by lidar and OPC were conducted on 24 April and 29 May. Cloud heights measured by lidar are hundreds of meters higher than those measured by the OPC, probably due to spatial variation in cloud height as the OPC moves tens kilometers from the launch site by wind. Note that this height difference is not due to the instrumental error because lidar measurements of cloud heights below 15 km are not always higher than those recorded by the OPC (data not shown). In addition, Fig. 5 of Peter et al. (2003) and Fig. 7 of Martucci et al. (2006) show an air-borne lidar measurement that cloud height at TT was also different about hundreds meter within tens km even though the cloud was geometrically thin cirrus. Therefore, cirrus cloud

Title Page

Abstract

Introduction

Conclusions

References

Tables

Figures

◀

▶

◀

▶

Back

Close

Full Screen / Esc

Printer-friendly Version

Interactive Discussion

height at TT is varied.

It is assumed for the present purposes that the cloud microphysics measured simultaneously by the lidar and OPC at the TT are the same; hence, the microphysical values presented below are therefore estimates.

5 Because the number concentration N is given by the OPC for particle radii greater than $3.4\ \mu\text{m}$, and β is given by lidar, the mode radius r_g or standard deviation σ_g of the particle size distribution can be obtained assuming the size distribution of cloud particles to be log-normal as follows.

$$\frac{dn}{dr} = \frac{N}{\sqrt{2\pi} \ln \sigma_g} \frac{1}{r} \exp \left[- \left(\frac{\ln r - \ln r_g}{\sqrt{2} \ln \sigma_g} \right)^2 \right]. \quad (5)$$

10 Mie theory (Bohren and Huffman, 1998) is applied for the analysis and the reason is as follows: It is impossible at present to calculate the backscattering cross section of irregularly shaped particles with size parameter ($=2\pi r/\lambda$, radius r and wavelength λ) of greater than approximately 50 due to the limitations of computer power. Therefore, an approximation is required for the analysis. Iwasaki and Okamoto (2001) estimated backscattering on the basis of Kirchhoff's diffraction theory, and showed that
15 the backscattering of $20\ \mu\text{m}$ plate-like particles with horizontally random orientation is expected to be one order of magnitude larger than for spherical particles. However, as this orientation is rare, and randomly oriented particles produce similar signals as spheres.

20 Assuming σ_g of 1.6, the maximum r_g is estimated to be $3.6\ \mu\text{m}$ for the clouds detected on April 24, and $11.2\ \mu\text{m}$ for May 29. Here, N is 3.2×10^4 and 5.9×10^3 / m^3 at the TT, and $\beta(532)$ is 2.4×10^{-7} and 4.0×10^{-7} / m/str , respectively.

Particle size distributions in the tropical tropopause

S. Iwasaki et al.

Title Page

Abstract

Introduction

Conclusions

References

Tables

Figures

◀

▶

◀

▶

Back

Close

Full Screen / Esc

Printer-friendly Version

Interactive Discussion

4 Discussion

Since smaller particles ($<1 \mu\text{m}$ radius) are liquid particles, corresponding to the known Junge layer, while particles larger than $3.4 \mu\text{m}$ in radius are ice particles (Appendix B), it is considered that liquid particles are frozen in the intermediate size range. Hayashi et al. (1998) showed that enhancement in the integrated number of particles on the largest channel ($r > 1.8 \mu\text{m}$) indicates polar stratospheric clouds (PSCs) consisting of ice particles. By analogy with the PSC study, the results in Fig. 3 suggest that liquid particles tend to be frozen at approximately $r > 0.7 \mu\text{m}$. Therefore, the enhancement is one of the keys to reveal frozen process at TT.

The ratio of $\sigma(\text{counts})$ to $\sigma(\text{Poisson})$ for ice clouds is different from that in cloud-free cases where the ratio reflects the vertical homogeneity of the particle number concentration. Thus it is a good indicator of the presence of ice particles. In addition, this ratio has a peak from $0.5 \mu\text{m}$ to $1.7 \mu\text{m}$ when cirrus clouds are present at the TT (Fig. 4d), but not at heights of 10–15 km (Fig. 4b). This characteristic, indicating non-uniformity of the vertical profile of particle numbers in this size range, is thus a typical feature of cirrus clouds in the TT. The non-uniformity implies that particles in this size range are actively frozen, so that the timing of freezing varies with height in the TT.

Figure 5 shows that cirrus clouds at 10–15 km were detected on 7 OPC launches, and in 6 cases cirrus clouds were detected at the TT. Only once was a local maximum detected in the particle size distribution at $2.0 \mu\text{m}$ at 10–15 km, while in 4 cases the maximum was observed in the TT. This result suggests that the speed of cloud growth below 15 km is much higher than that at the cold-point temperature, and the transition from liquid to ice is less observable since the mixing ratio is higher at warmer temperatures. For example, the growth times of ice particles of radius from 0.1 to $3 \mu\text{m}$ at -60 and -80°C are 40 s and 13 min under a relative humidity with respect to ice (RH_i) of 120% (see Appendix B). Once liquid particles are frozen, a gap forms in the size distribution due to the Bergeron-Findeisen process (e.g., Emanuel, 1994); this gap is observed at $2.9 \mu\text{m}$ on three launches at 10–15 km and two launches at TT.

Particle size distributions in the tropical tropopause

S. Iwasaki et al.

Title Page

Abstract

Introduction

Conclusions

References

Tables

Figures

◀

▶

◀

▶

Back

Close

Full Screen / Esc

Printer-friendly Version

Interactive Discussion

Particle size distributions in the tropical tropopause

S. Iwasaki et al.

[Title Page](#)[Abstract](#)[Introduction](#)[Conclusions](#)[References](#)[Tables](#)[Figures](#)[◀](#)[▶](#)[◀](#)[▶](#)[Back](#)[Close](#)[Full Screen / Esc](#)[Printer-friendly Version](#)[Interactive Discussion](#)

A very narrow ice particle size distribution generally indicates that the ice crystals have a similar history (i.e., formed at the same time), whereas a broader ice particle size distribution indicates that the particles may have formed at different times and different locations. The local maximum of dn/dr at $2.0\ \mu\text{m}$ at the TT may therefore indicate that all observed particles were generated by the same mechanism.

As enhancement in the integrated number concentration was observed on most launches when cirrus clouds were detected at 10–15 km and at TT, and the peak of $\sigma(\text{counts})/\sigma(\text{Poisson})$ and the local maximum in dn/dr are common for some cirrus clouds at the TT at least during the present observational period, the size distributions at $0.5\text{--}3\ \mu\text{m}$ are considered to be characteristic of cirrus clouds in the TTL. Computer simulations of thin cirrus clouds in the TTL are thus expected to be consistent with these observations.

5 Summary

A total of 11 OPC launches were conducted in Thailand from April to June 2003. On 6 occasions, cirrus clouds were detected at the tropical tropopause, 4 of which were immediately prior or following the monsoon onset in late May. These results indicate that a cirrus cloud in TT tends to occur in association with nearby deep convection. The particle sizes measured by the OPC were re-calculated by the FDTD method in order to account for observation error induced by irregularly shaped particles. Lidar observations were conducted simultaneously, and comparison of the lidar cloud heights with the OPC results indicates that the cloud height is variable by several hundreds meters over tens kilometers, despite the huge horizontal scale ($\sim 500\ \text{km}$; Winker and Trepte, 1998) and geometrical thinness of such clouds. The mode radius of particles in clouds was estimated to be less than approximately $10\ \mu\text{m}$ on the basis of both OPC and lidar data. For example, the maximum mode radii for clouds detected on April 24 and May 29 are estimated to be $3.6\ \mu\text{m}$ and $11.2\ \mu\text{m}$ assuming a standard deviation as $1.6\ \mu\text{m}$.

Particle size distributions in the tropical tropopause

S. Iwasaki et al.

[Title Page](#)[Abstract](#)[Introduction](#)[Conclusions](#)[References](#)[Tables](#)[Figures](#)[◀](#)[▶](#)[◀](#)[▶](#)[Back](#)[Close](#)[Full Screen / Esc](#)[Printer-friendly Version](#)[Interactive Discussion](#)

Enhancements in the integrated number concentration and $\sigma(\text{counts})/\sigma(\text{Poisson})$ ratio were found to be good indicators of the presence of ice particles to reveal frozen process at TT. The increase in the σ ratio from $0.5\ \mu\text{m}$ to $1.7\ \mu\text{m}$ is a typical feature of cloud particles in the TT, and implies that particles in this size range are actively frozen, so that the timing of freezing varies with height in the TT.

Comparisons of the average particle size distributions in the presence and absence of cirrus clouds at the TT revealed that all ice particles in the clouds may be nucleated by the same mechanism based on the local maximum of the size distribution at $2.0\ \mu\text{m}$ in the TT.

As these features are common and particular to cirrus clouds, the characteristic size distributions for particle radii of $0.5\text{--}3.0\ \mu\text{m}$ obtained in this study should also be seen in ice nucleation studies and computer simulations of thin cirrus clouds at the TT. The present study thus yields some interesting results pertaining to ice nucleation, and demonstrates that OPCs are effective for observing both aerosols and the generation mechanism of cirrus clouds in the TTL. A comparison of OPC data with parcel model results will be presented as part of future validation of the present results.

Acknowledgements. Parts of this study were supported by the Research Institute for Humanity and Nature (RIHN), Kyoto, Japan and by the Core Research for Evolutional Science and Technology (CREST) program of Japan Science and Technology Agency (JST). The data used in this study were obtained as a part of the Coordinated Enhanced Observing Period (CEOP) activity.

Appendix A

Size error in OPC data

The OPC counts numbers of particles by using eight ΔC_{sca} thresholds, as shown in Fig. 6, where ΔC_{sca} is calculated by Mie theory and the FDTD method; e.g., channel 1 counts particles with ΔC_{sca} greater than $0.003\ \mu\text{m}^2$. The size error introduced by

Particle size distributions in the tropical tropopause

S. Iwasaki et al.

Title Page

Abstract

Introduction

Conclusions

References

Tables

Figures

◀

▶

◀

▶

Back

Close

Full Screen / Esc

Printer-friendly Version

Interactive Discussion

the various irregularly shaped particles is estimated as follows. Four shapes of particles are examined. In Fig. 6, “Sphere” denotes spherical sulfuric acid particles with refractive index of $1.4+i0$ or water ice ($1.3+i0$; Warren, 1984). Model A denotes an 8-hexagonal aggregate defined in Yang and Liou (1998), model B is the same but with all distances of barycenters half that of model A, as defined in Ishimoto and Kobayashi (2006), and model C denotes a hexagonal column with aspect ratio of 1.7, where the ratio is defined as $2R/L$ with R and L being the lengths of one side of the hexagon and the column. Each irregularly shaped particle is randomly oriented and the refractive index is set to that of water ice. Hence, the observation error is due to both non-sphericity of the ice particles and the difference in refractive index.

Ishimoto and Kobayashi (2006) showed that scattering by model A is similar to the average scattering by individual hexagonal columns in the aggregate, while scattering by model B contains lots of interference of scattering by 8 hexagonal columns. That is, models A and B not only show the scattering by themselves but also represent the average scattering related to variously shaped hexagonal columns (model A) and complex-shaped particles (model B).

To obtain modified r and the error bars in r , we average radius at each channel and calculate the standard deviations. Moreover, since there are error bars in each radius, dn/dr also has error bars. To determine modified dn/dr and its error bar, we average each dn/dr and calculate the standard deviations.

Appendix B

Growth rates of liquid and ice

The liquid and ice particle growth rates are calculated by the following equations, where r_w and r_i denote the radii of liquid and ice particles and t denotes time. All symbols

are the same as those described in the Appendix of Spice et al. (1999).

$$\frac{dr_w}{dt} = \frac{1}{\rho_w r_w} \left(\sigma_w - \frac{b}{T r_w} + \frac{cm_s}{r_w^3} \right) \left[\frac{R_u}{e_{s,w} D_a' M_w} + \frac{L_v}{K_a' T} \left(\frac{L_v M_w}{R_u} - 1 \right) \right]^{-1},$$

$$\frac{dr_i}{dt} = \frac{\sigma_i}{\rho_i r_i} \left[\frac{R_u}{e_{s,i} D_a' M_w} + \frac{L_v}{K_a' T} \left(\frac{L_v M_w}{R_u} - 1 \right) \right]^{-1} \quad (B1)$$

Figure 7 shows the growth rate for particles of radius from 0.1 to 3 μm at -80°C , where the particle phase (liquid or ice) does not change. The molalities (number of moles of dissociated solute per unit mass of solvent) of water ice and sulfuric acid (liquid) are 0.1 and 10, respectively. As RHi and the ambient temperature are assumed to be constants, the graph shows the fastest growing rates. From Fig. 7, liquid particles can grow when RHi is greater than 195%, since the relative humidity with respect to water RHw is lower than RHi. The results for $(\text{NH}_4)_2\text{SO}_4$ also show similar results (data not shown). However, the value is not realistic (e.g., Jensen et al., 2001, Fig. 5). Hence, liquid particles of the Junge layer, cannot grow up to 3 μm without freezing, indicating that such large particles must be ice particles.

References

- Baumgardner, D., Dye, J. E., Gandrud, B., Barr, K., Kelly, K., and Chan, K. R.: Refractive indices of aerosols in the upper troposphere and lower stratosphere, *Geophys. Res. Lett.*, 23, 749–752, 1996.
- Boehm, M. T. and Verlinde, J.: Stratospheric influence on upper tropospheric tropical cirrus, *Geophys. Res. Lett.*, 27, 3209–3212, 2000.
- Bohren, C. F. and Huffman, D. R.: Absorption and scattering of light by small particles, Wiley-Interscience, 530 pp., 1998.
- Comstock, J. M., Ackerman, T. and Mace, G. G.: Ground-based lidar and radar remote sensing of tropical cirrus clouds at Nauru Island: Cloud statistics and radiative impacts, *J. Geophys. Res.*, 107(D23), 4714, doi:10.1029/2002JD002203, 2002.

Particle size distributions in the tropical tropopause

S. Iwasaki et al.

Title Page

Abstract

Introduction

Conclusions

References

Tables

Figures

◀

▶

◀

▶

Back

Close

Full Screen / Esc

Printer-friendly Version

Interactive Discussion

**Particle size
distributions in the
tropical tropopause**S. Iwasaki et al.

[Title Page](#)[Abstract](#)[Introduction](#)[Conclusions](#)[References](#)[Tables](#)[Figures](#)[◀](#)[▶](#)[◀](#)[▶](#)[Back](#)[Close](#)[Full Screen / Esc](#)[Printer-friendly Version](#)[Interactive Discussion](#)

Eguchi, N. and Shiotani, M.: Intraseasonal variations of water vapor and cirrus clouds in the tropical upper troposphere, *J. Geophys. Res.*, 109(D12106), doi:10.1029/2003JD004314, 2004.

Emanuel, K. A.: *Atmospheric Convection*, Oxford Univ. Press, New York, 1994.

5 Gettelman, A., Forster, P. M. de F., Fujiwara, M., Fu, Q., Vomel, H., Gohar, L. K., Johanson, C., and Ammerman, M.: Radiation balance of the tropical tropopause layer, *J. Geophys. Res.*, 109, D07103, doi:10.1029/2003JD004190, 2004.

Hasebe, F., Shiotani, M., Fujiwara, M., Dunkerton, T. J., Folkins, I., Fortuin, P., Gettelman, A., Hashiguchi, N. O., Iwasaki, S., Kasai, Y., Nishi, N., Niwano, M., Oltmans, S., Poveda, L.,
10 Randel, W., Rosenlof, K., Tsushima, Y., Vömel, H., and Yamazaki, K.: Report of the 2nd International SOWER Meeting, SPARC Newsletter, 24, 21–27, 2005.

Hayashi, M., Iwasaka, Y., Watanabe, M., Shibata, T., Fujiwara, M., Adachi, H., Sakai, T., Nagatani, M., Gernandt, G., Neuber, R., and Tsuchiya, M.: Size and number concentration of liquid PSCs: Balloon-borne measurements at Ny-Alesund, Norway in winter of 1994/95, *J.*
15 *Meteorol. Soc. Japan*, 76, 549–560, 1998.

Hobbs, P. V.: *Introduction to Atmospheric Chemistry*, Cambridge Univ. Press, Cambridge, p.179, 2000.

Ishimoto, H. and Kobayashi, T.: Effect of minor deformation for the light scattering of ice and aerosol particles, *Proc. SPIE*, 6408, 64081B, 2006.

20 Iwasaki, S. and Okamoto, H.: Analysis of the enhancement of backscattering by nonspherical particles with flat surfaces, *Appl. Opt.*, 40, 6121–6129, 2001.

Iwasaki, S., Tsushima, Y., Shirooka, R., Katsumata, M., Yoneyama, K., Matsui, I., Shimizu, A., Sugimoto, N., Kamei, A., Kuroiwa, H., Kumagai, H., and Okamoto, H.: Subvisual cirrus cloud observations using a 1064-nm lidar, a 95 GHz cloud radar, and radiosondes in the warm
25 pool region, *Geophys. Res. Lett.*, 31, doi:10.1029/2003GL019377, 2004.

Jensen, E. J., Toon, O. B., Selkirk, H. B., Spinhirne, J. D., and Schoeberl, M. R.: On the formation and persistence of subvisual cirrus clouds near the tropical tropopause, *J. Geophys. Res.*, 101, 21 361–21 375, 1996.

Jensen, E. J., Pfister, L., Ackerman, A. S., and Tabazadeh, A.: A conceptual model of the dehydration of air due to freeze-drying by optically thin, laminar cirrus rising slowly across the
30 tropical tropopause, *J. Geophys. Res.*, 106, 17 237–17 252, 2001.

Jensen, E. J., and Pfister, L.: Transport and freeze-drying in the tropical tropopause layer, *J. Geophys. Res.*, 109, doi:10.1029/2003JD004022, 2004.

**Particle size
distributions in the
tropical tropopause**

S. Iwasaki et al.

Title Page

Abstract

Introduction

Conclusions

References

Tables

Figures

◀

▶

◀

▶

Back

Close

Full Screen / Esc

Printer-friendly Version

Interactive Discussion

Kojima, T., Buseck, P. R., Wilson, J. C., Reeves, J. M., and Mahoney, M. J.: Aerosol particles from tropical convective systems: Cloud tops and cirrus anvils, *J. Geophys. Res.*, 109, D12201, doi:10.1029/2003JD004504, 2004.

Lynch, D. K., Sassen, K., Starr, D. O'C., and Stephens, G.: *Cirrus*, Oxford University Press, New York, 2002.

Martucci, G., Matthey, R., Mitev, V., Fix, A., and Kiemle, C.: Detection of ultra-thin tropical cirrus during TROCCINOX – A case study performed by two airborne lidars, *Proc. of 23rd International laser radar conference*, 585–588, 2006.

Matsuura, H.: A study on the cirrus variations near the tropical tropopause layer (TTL) by lidar measurement, M. S. thesis, Kyoto Univ., Japan, 31 March (in Japanese), 2005.

Peter, Th., Luo, B. P., Wirth, M., Kiemle, C., Flentje, H., Yushkov, V. A., Khattatov, V., Rudakov, V., Thomas, A., Borrmann, S., Toci, G., Mazzinghi, P., Beuermann, J., Schiller, C., Cairo, F., Donfrancesco, G. Di, Adriani, A., Volk, C. M., Strom, J., Noone, K., Mitev, V., MacKenzie, R. A., Carslaw, K. S., Trautmann, T., Santacesaria, V., and Stefanutti, L.: Ultrathin Tropical Tropopause Clouds (UTTCs): I. Cloud morphology and occurrence, *Atmos. Chem. Phys.*, 3, 1083–1091, 2003,

<http://www.atmos-chem-phys.net/3/1083/2003/>.

Sassen, K. and Cho, B. S.: Subvisible-thin cirrus lidar dataset for satellite verification and climatological research, *J. Appl. Meteorol.*, 31, 1275–1285, 1992.

Spice, A., Johnson, D. W., Brown, P. R. A., Darlison, A. G., and Saunders, C. P. R.: Primary ice nucleation in orographic cirrus cloud: A numerical simulation of the microphysics, *Q. J. R. Meteorol. Soc.*, 125, 1637–1667, 1999.

Steele, H. M. and Hamill, P.: Effects of temperature and humidity on the growth and optical properties of sulfuric acid–water droplets in the stratosphere, *J. Aerosol Sci.*, 12, 517–528., 1981.

Tsuchiya, M., Kasai, T., Hayashi, M., Iwasaka, Y., and Takami, K.: Development of aerosol sonde for observation balloon, *Keisoku Jidouseigy Gakkai Ronbunshu*, 32, 290–296 (in Japanese), 1996.

Yang, P. and Liou, K. N.: Light scattering by hexagonal crystals: Comparison of finite difference time domain method, *J. Opt. Soc. Am.*, 12, 162–176, 1995.

Yang, P. and Liou, K. N.: Single-scattering properties of complex ice crystals in terrestrial atmosphere, *Contr. Atmos. Phys.*, 71, 223–248, 1998.

Wang, P. H., Minnis, P., McCormick, M. P., Kent, G. S., and Skeens, K. M.: A 6-year climatology

of cloud occurrence frequency from stratospheric aerosol and gas experiment II observations (1985–1990), J. Geophys. Res., 101, 29 407–29 430, 1996.

Warren, S. G.: Optical constants of ice from the ultraviolet to the microwave. Appl. Opt., 23, 1206–1225, 1984.

- 5 Winker, D. M. and Trepte, C. R.: Laminar cirrus observed near the tropical tropopause by LITE, Geophys. Res. Lett., 25, 3351–3354, 1998.

ACPD

7, 1595–1622, 2007

**Particle size
distributions in the
tropical tropopause**

S. Iwasaki et al.

Title Page

Abstract

Introduction

Conclusions

References

Tables

Figures

⏪

⏩

◀

▶

Back

Close

Full Screen / Esc

Printer-friendly Version

Interactive Discussion

EGU

Table 1. Specification of balloon-borne optical particle counter.

Dimension (L×W×H):	25×38×31 cm
Weight:	3.5 kg (including battery)
Light source:	Laser diode
wavelength	$\lambda=780$ nm (70 mW of output)
Detection:	Lateral scattering light with a photodiode
Angle of collecting axis	60° from source light
Width of collecting area	44° of half solid angle
Sampling flow rate:	50 cm ³ /s (at ground level condition)
Particle counting:	8 channel parallel counter *
Integrating duration:	16 s
Data transmission:	Narrow FM (model RS-01G, MEISEI Elec. Co. Ltd)
Carrier wave:	400 MHz (model RS-01G, MEISEI Elec. Co. Ltd)
Modulation:	FSK (Bell103 2025/2225 Hz)

* In the case of spherical sulfuric acid particles, each channel counts the numbers of particles with radii greater than 0.15, 0.25, 0.40, 0.60, 1.0, 1.7, 2.5, and 3.5 μm . In the case of irregularly shaped particles, the equivalent radii r_{eq} in each channel are 0.18±0.01, 0.30±0.03, 0.48±0.05, 0.70±0.06, 0.99±0.01, 1.65±0.18, 2.44±0.28, and 3.35±0.34 μm , respectively (see Appendix A).

Particle size distributions in the tropical tropopause

S. Iwasaki et al.

Title Page

Abstract

Introduction

Conclusions

References

Tables

Figures

◀

▶

◀

▶

Back

Close

Full Screen / Esc

Printer-friendly Version

Interactive Discussion

Table 2. Particle numbers and $\beta_{\text{MAX}}(532)$ measured with the OPCs and the lidar at TT.

OPC		Lidar
Launched time (UT)	Number on channel 8 [m^3] Height [km], Temperature [$^{\circ}\text{C}$]	$\beta_{\text{MAX}}(532)$ [m/str] Height [km]
06:46, 26 March	–	–
22:00, 26 March	–	–
03:50, 27 March	$4.5 \times 10^3 / \text{m}^3$ 17.7 km, -77.7°C	–
06:14, 23 April	–	–
03:17, 24 April	$3.2 \times 10^4 / \text{m}^3$ 16.9 km, -78.6°C	$2.4 \times 10^{-7} / \text{m}/\text{str}$ 17.1–17.3 km
18:23, 25 April	–	–
14:17, 26 April	–	–
06:59, 29 May	$5.9 \times 10^3 / \text{m}^3$ 16.5–16.9 km, -80.0 to -82.0°C	$4.0 \times 10^{-7} / \text{m}/\text{str}$ 17.0–17.2 km
12:26, 30 May	$4.2 \times 10^5 / \text{m}^3$ 16.8–18.3 km, -78.3 to -83.2°C	X
00:22, 01 June	$6.3 \times 10^4 / \text{m}^3$ 16.1–16.3 km, -77.0 to -77.4°C	X
07:15, 04 June	$6.5 \times 10^4 / \text{m}^3$ 16.6–17.3 km, -79.3 to -82.6°C	X

No entry indicates that no cirrus cloud was detected at the TT. X denotes cases in which lidar observation at the TT was not possible due to optically dense clouds below the TT. $\beta_{\text{MAX}}(532)$ denotes the maximum β at 532 nm in cirrus clouds at the TT.

Particle size distributions in the tropical tropopause

S. Iwasaki et al.

Title Page

Abstract

Introduction

Conclusions

References

Tables

Figures

◀

▶

◀

▶

Back

Close

Full Screen / Esc

Printer-friendly Version

Interactive Discussion

Particle size distributions in the tropical tropopause

S. Iwasaki et al.

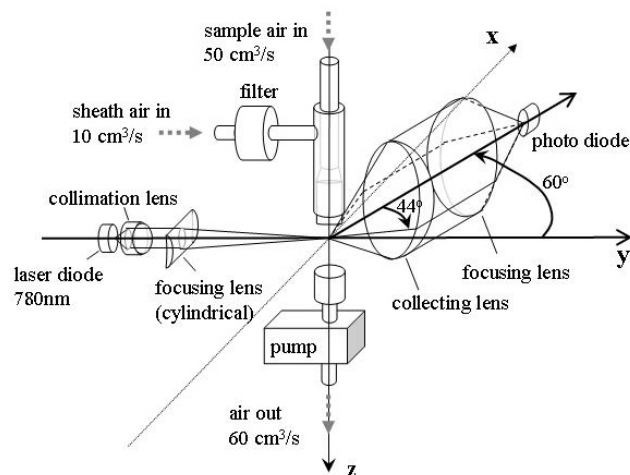


Fig. 1. Schematic diagram of OPC. Transmitted laser beams are linear-polarized parallel to the $x - y$ plane. The photo diode is on the $x - y$ plane.

[Title Page](#)[Abstract](#)[Introduction](#)[Conclusions](#)[References](#)[Tables](#)[Figures](#)[◀](#)[▶](#)[◀](#)[▶](#)[Back](#)[Close](#)[Full Screen / Esc](#)[Printer-friendly Version](#)[Interactive Discussion](#)

**Particle size
distributions in the
tropical tropopause**

S. Iwasaki et al.

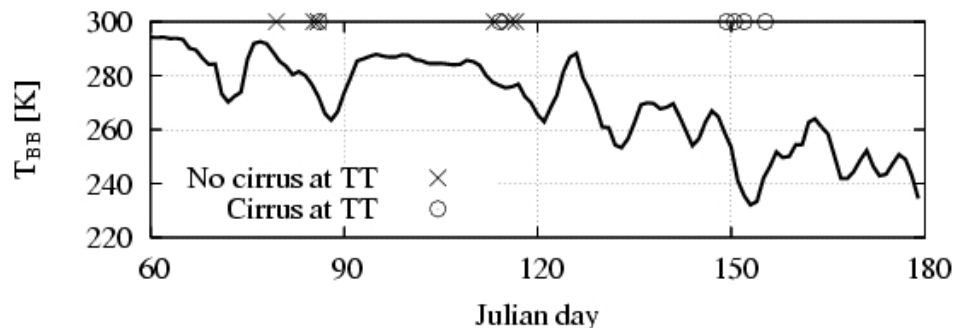


Fig. 2. Black body temperature (T_{BB}) over the observation site averaged over the range $17.16\pm 0.5^\circ\text{N}$, $99.87\pm 0.5^\circ\text{E}$ for 2 days. “O” denotes OPC launches on which cirrus cloud was detected at the TT, and “X” denotes cases where no cloud was detected.

[Title Page](#)[Abstract](#)[Introduction](#)[Conclusions](#)[References](#)[Tables](#)[Figures](#)[◀](#)[▶](#)[◀](#)[▶](#)[Back](#)[Close](#)[Full Screen / Esc](#)[Printer-friendly Version](#)[Interactive Discussion](#)

Particle size distributions in the tropical tropopause

S. Iwasaki et al.

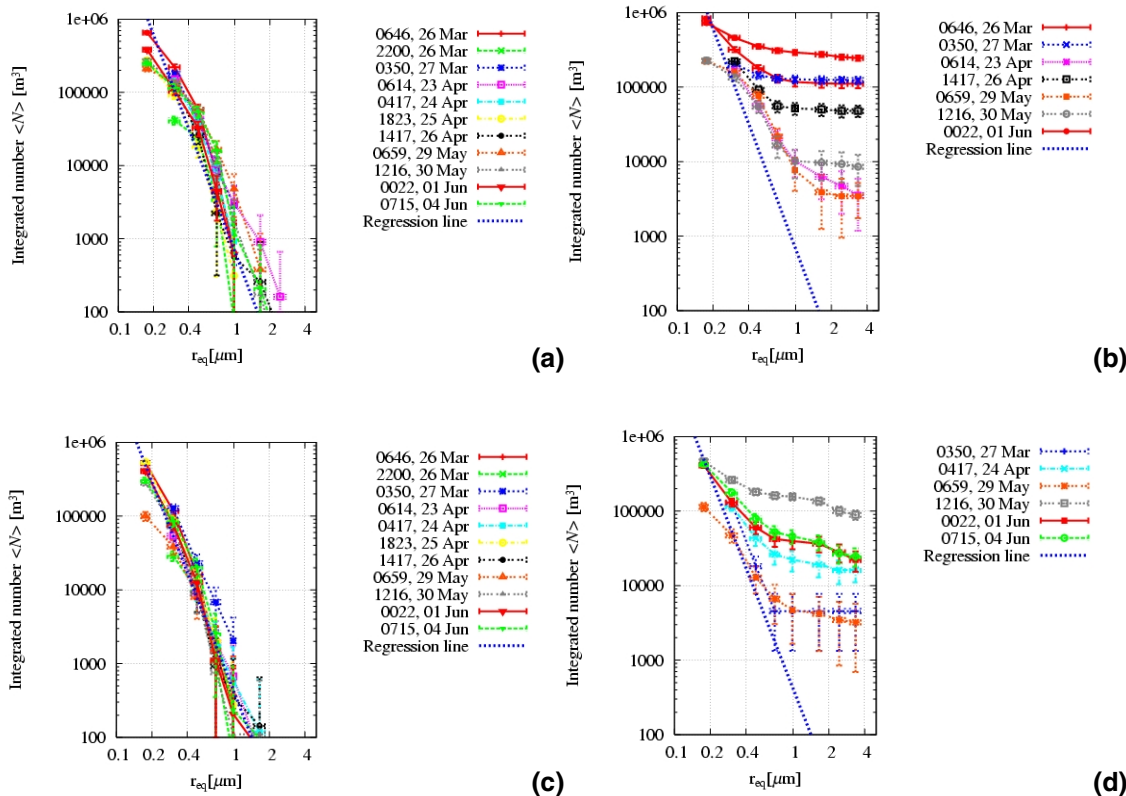


Fig. 3. Integrated number of particles (**a**, **b**) at 10–15 km and (**c**, **d**) at the TT (<-75 °C) under conditions of (a,c) no cloud (background aerosols) and (b,d) cloud. Regression lines are $6.7 \times 10^2 r^{-4.2} / \text{m}^3$ in (a), and $4.1 \times 10^2 r^{-4.1} / \text{m}^3$ in (c), and both lines are also drawn in (b) and (d), respectively. Error bars at equivalent radius r_{eq} are calculated by the scattering of irregularly shaped particles as explained in Appendix A, while error bars at $\langle N \rangle$ are standard deviations of the Poisson distribution.

Title Page

Abstract

Introduction

Conclusions

References

Tables

Figures

◀

▶

◀

▶

Back

Close

Full Screen / Esc

Printer-friendly Version

Interactive Discussion

Particle size distributions in the tropical tropopause

S. Iwasaki et al.

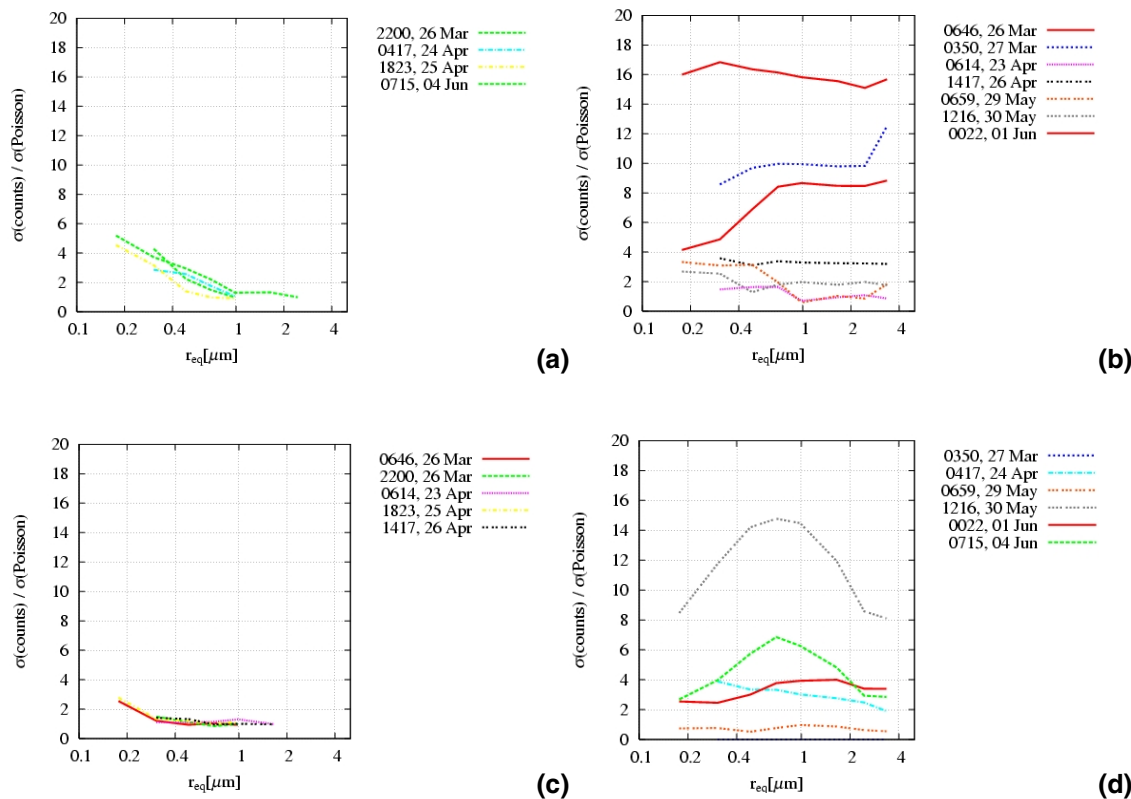


Fig. 4. Ratio of standard deviation of counts (raw data) to that of the Poisson distribution of average counts (**a**, **b**) at 10–15 km and (**c**, **d**) at the TT (<-75 °C) under conditions of (a, c) no cloud (background aerosols) and (b, d) cloud.

Title Page

Abstract Introduction

Conclusions References

Tables Figures

◀ ▶

◀ ▶

Back Close

Full Screen / Esc

Printer-friendly Version

Interactive Discussion

Particle size distributions in the tropical tropopause

S. Iwasaki et al.

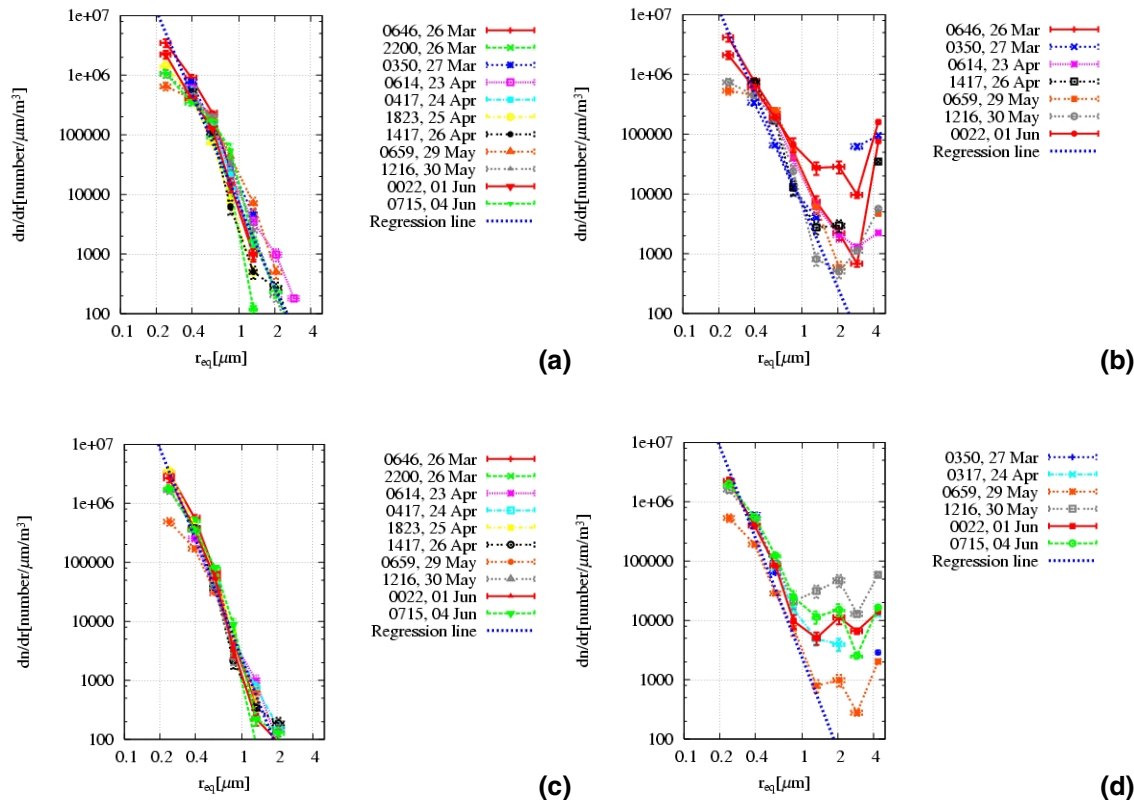


Fig. 5. Averaged particle size distributions (**a, b**) at 10–15 km and (**c, d**) at the TT ($<-75^\circ\text{C}$) under conditions of (a, c) no cloud (background aerosols) and (b, d) cloud.

Title Page

Abstract

Introduction

Conclusions

References

Tables

Figures

◀

▶

◀

▶

Back

Close

Full Screen / Esc

Printer-friendly Version

Interactive Discussion

Particle size distributions in the tropical tropopause

S. Iwasaki et al.

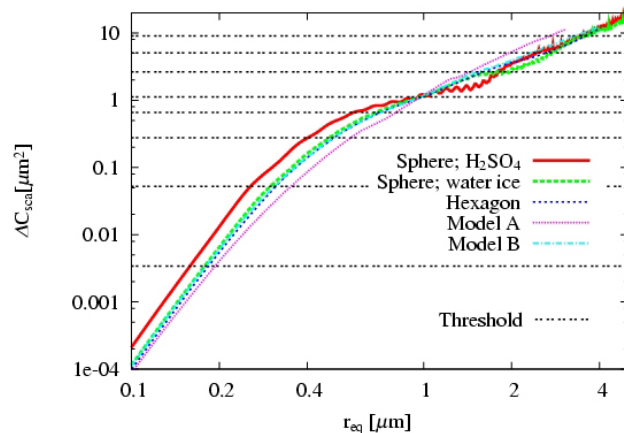


Fig. 6. ΔC_{sca} (μm^2) at 60° scattering angle with 44° half solid angle calculated by Mie theory and the FDTD method. Equivalent radius r_{eq} is defined as $(3V/4\pi)^{1/3}$, where V is particle volume. Threshold values for ΔC_{sca} in each channel are shown.

Title Page

Abstract

Introduction

Conclusions

References

Tables

Figures

◀

▶

◀

▶

Back

Close

Full Screen / Esc

Printer-friendly Version

Interactive Discussion

**Particle size
distributions in the
tropical tropopause**

S. Iwasaki et al.

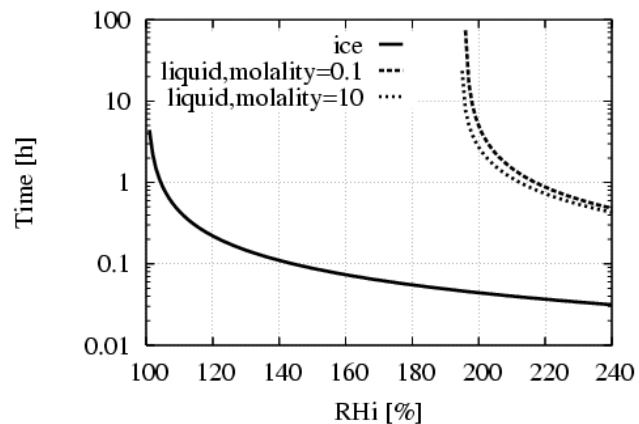


Fig. 7. Growth time for particles of radii from 0.1 to 3 μm at -80°C . RH_i and ambient temperature are constant.

[Title Page](#)[Abstract](#)[Introduction](#)[Conclusions](#)[References](#)[Tables](#)[Figures](#)[◀](#)[▶](#)[◀](#)[▶](#)[Back](#)[Close](#)[Full Screen / Esc](#)[Printer-friendly Version](#)[Interactive Discussion](#)